Supplementary Information

$CaIn_2S_4$-In_2O_3 hybrid nanofibers with expedited photocarrier separation for fast photocatalytic bacterial inactivation under visible light

Lina Wang[a, c]‡, Zhiping Wan[b]‡, Xiaoxiang Xu[a,c]*, and Jun Qian[b]*

[a]*Shanghai Key Lab of Chemical Assessment and Sustainability, School of Chemical Science and Engineering, Tongji University, Shanghai, 200092, China*

Email: xxxu@tongji.edu.cn

[b]*Department of Neurosurgery, Tongji Hospital, Tongji University School of Medicine, Tongji University, 389 Xincun Road, Shanghai, 200065, China*

Email:qianjun19@126.com

[c]*Clinical and Central Lab, Putuo People's Hospital, Tongji University, Shanghai, 200060, China*

* Corresponding authors

‡ These authors contributed equally.

Supplementary information content

Number of pages: 12 (S1-S12)

Number of figures: 12 (Figure S1-S12)

Number of Tables: 2 (Table S1-S2)

Contents

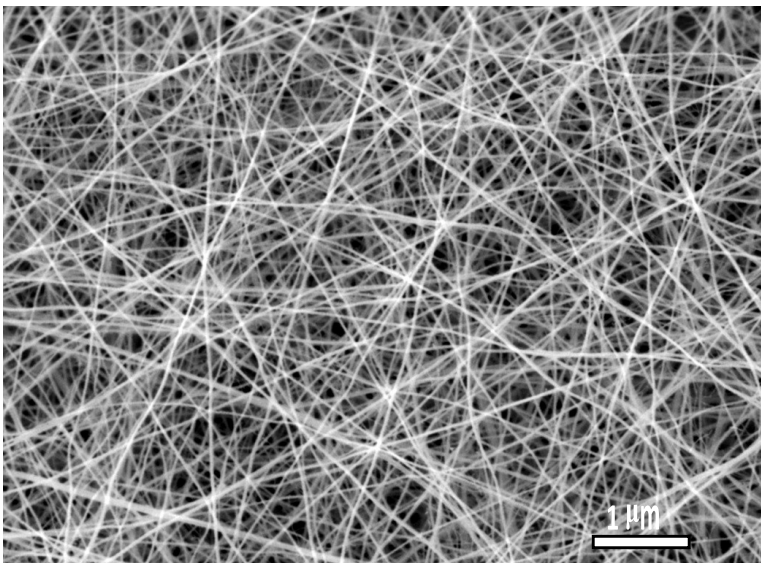

Figure S1. FE-SEM image of as-prepared In_2O_3 fibers by the electrospinning method.

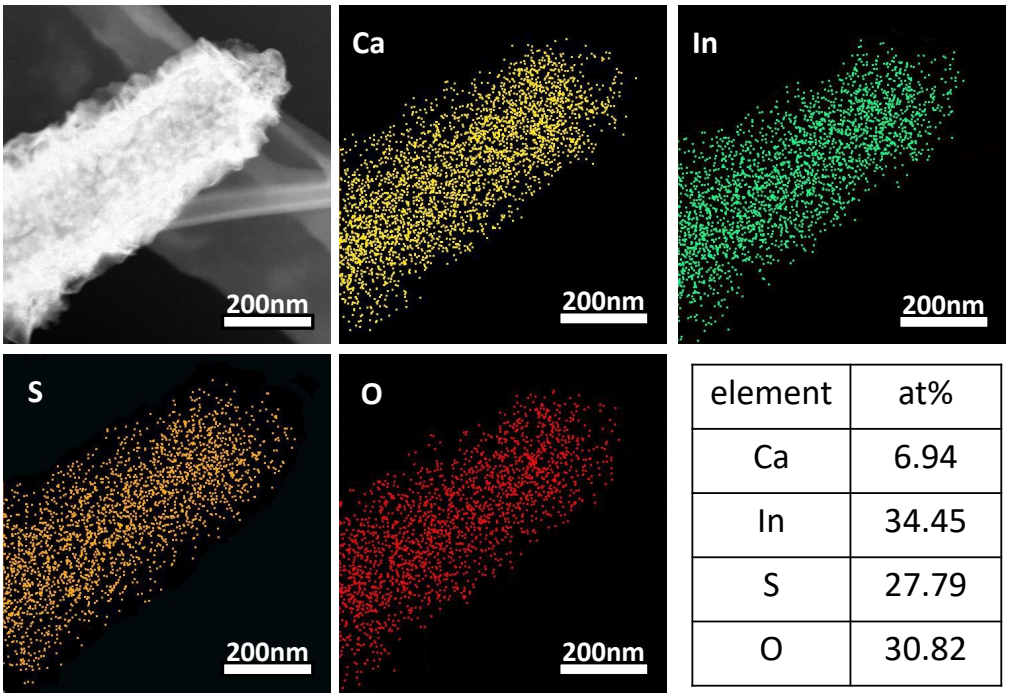

element	at%
Ca	6.94
In	34.45
S	27.79
O	30.82

Figure S2. SEM-EDS mapping of single $CaIn_2S_4$-In_2O_3 fiber, the element content is tabulated in the inset table.

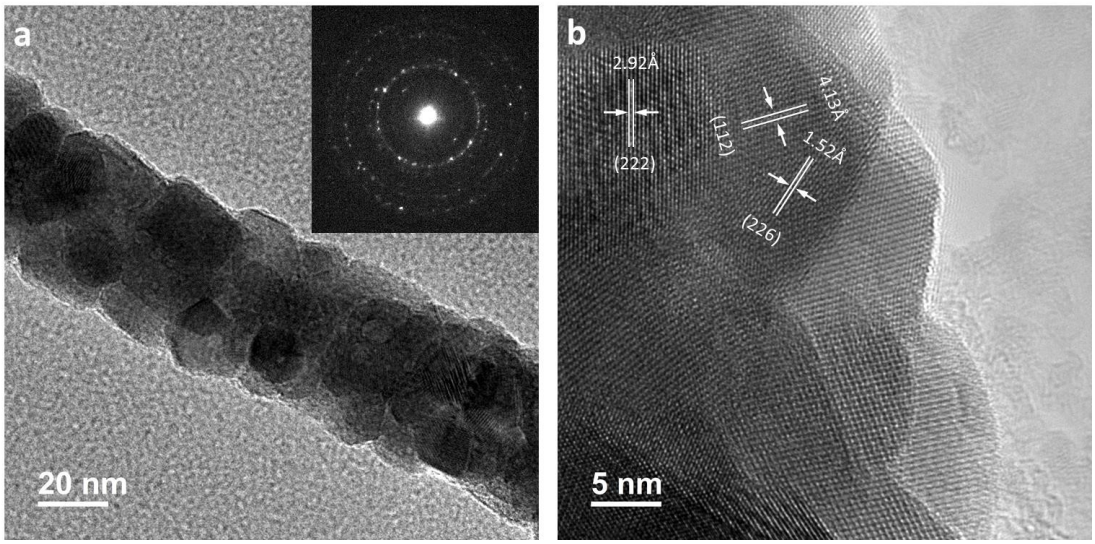

Figure S3. (a) TEM image of a single In_2O_3 fiber, inset shows the selected area electron diffraction patterns; (b) high resolution TEM image of a single In_2O_3 fiber, the lattice fringes marked correspond to (222), (112) and (226) planes of In_2O_3.

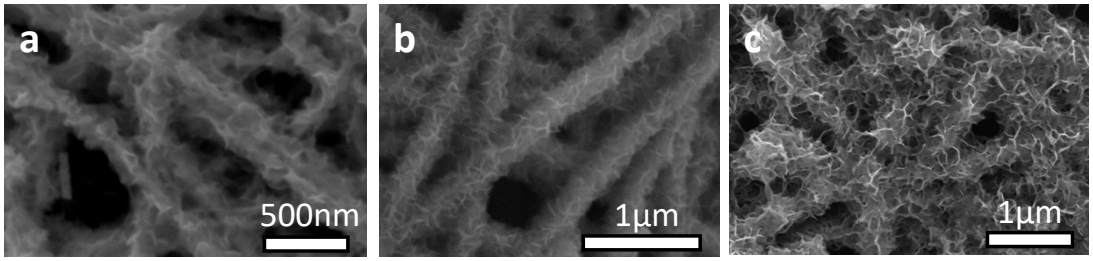

Figure S4. FE-SEM image of $CaIn_2S_4$-In_2O_3 fibers with different $CaIn_2S_4/In_2O_3$ molar ratio: (a) 1:2; (b) 1:1; (c) 2:1.

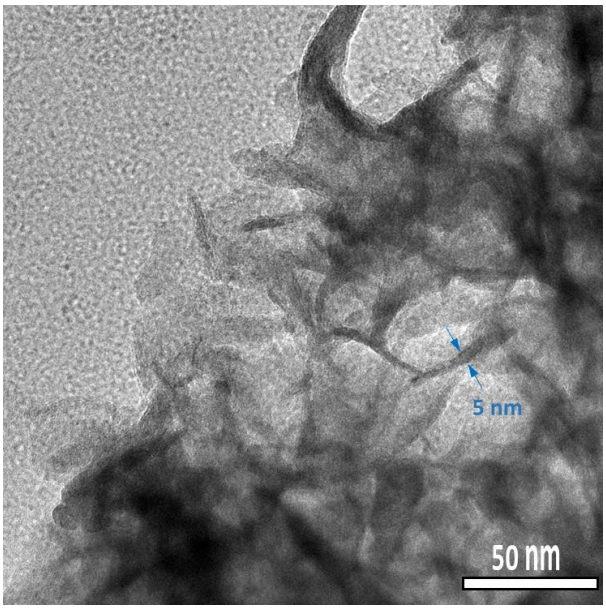

Figure S5. TEM image of $CaIn_2S_4$ nanofoils of the $CaIn_2S_4$-In_2O_3 fibers.

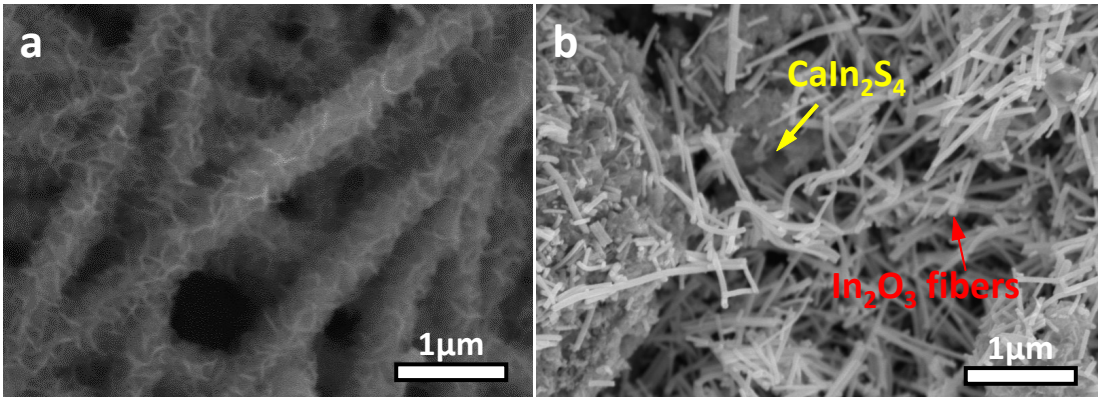

Figure S6. FE-SEM images of (a) $CaIn_2S_4$-In_2O_3 fibers; (b) $CaIn_2S_4$-In_2O_3 mixtures, the $CaIn_2S_4/In_2O_3$ molar ratio is fixed at 1:1.

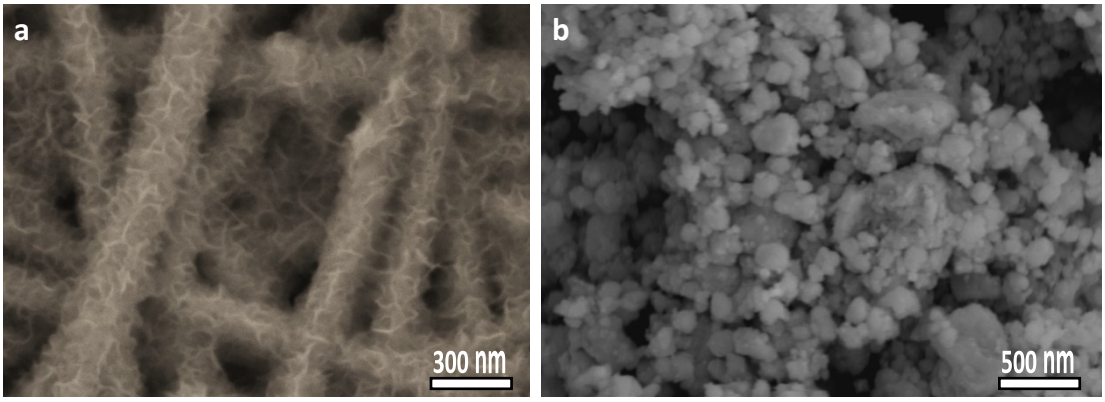

Figure S7. FE-SEM images of $CaIn_2S_4$-In_2O_3 fibers before and after mechanical grinding: (a) $CaIn_2S_4$-In_2O_3 fibers before grinding; (b) $CaIn_2S_4$-In_2O_3 debris after grinding.

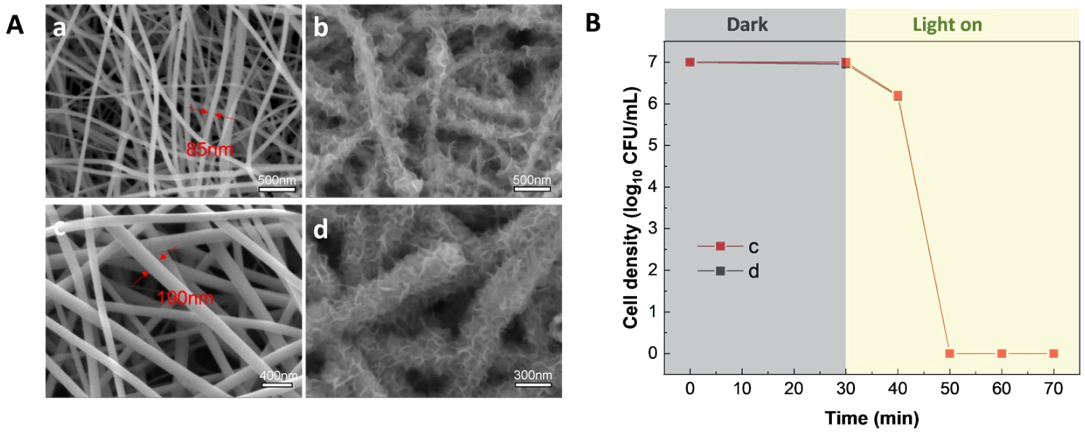

Figure S8. (A) FE-SEM images of In_2O_3 and $CaIn_2S_4$-In_2O_3 fibers with different aspect ratios: (a) In_2O_3 fibers with diameter of 85 nm; (b) $CaIn_2S_4$-In_2O_3 fibers prepared using In_2O_3 fibers with diameter of 85 nm; (c) In_2O_3 fibers with diameter of 190 nm; (d) $CaIn_2S_4$-In_2O_3 fibers prepared using In_2O_3 fibers with diameter of 190 nm. (B) Photocatalytic disinfection activity of $CaIn_2S_4$-In_2O_3 fibers with different aspect ratios from (A).

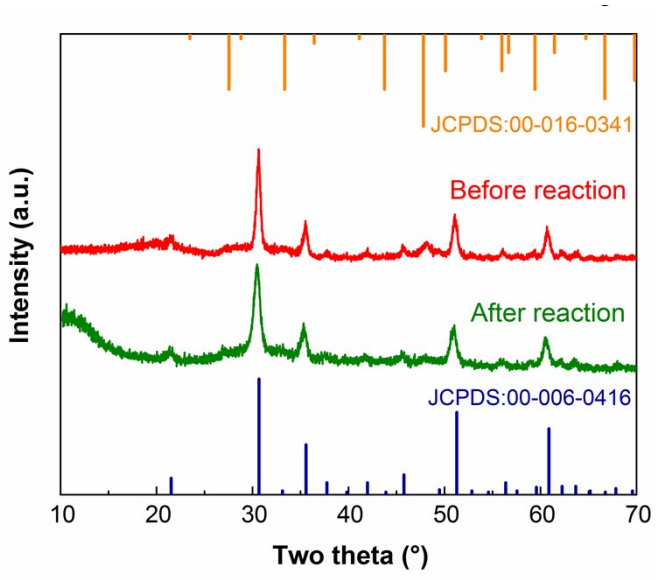

Figure S9. XRD patterns of $CaIn_2S_4$-In_2O_3 fibers before and after photocatalytic disinfection experiments.

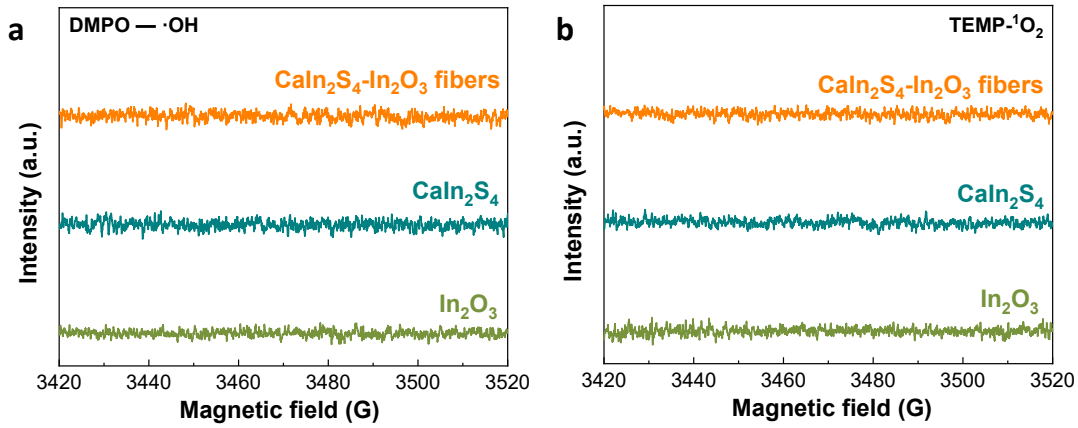

Figure S10. (a) DMPO spin-trapping EPR spectra for ·OH; (b) TEMP spin-trapping EPR spectra for $^1O_2$.

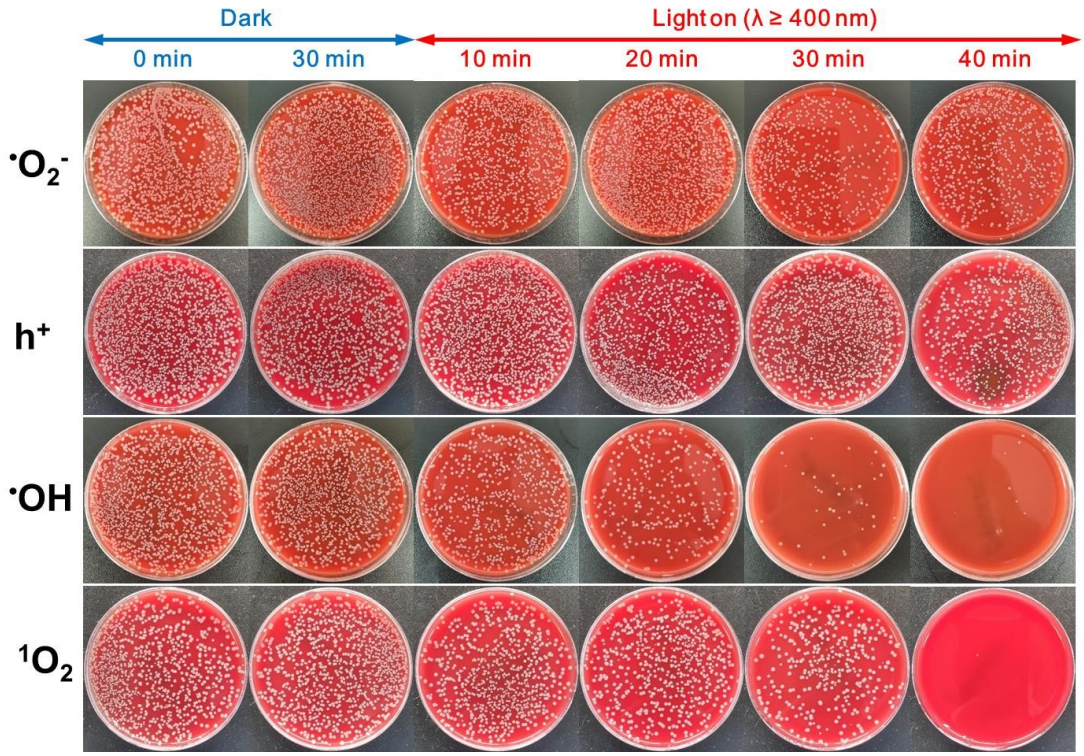

Figure S11. Bacterial colony growth results for illuminated $CaIn_2S_4$-In_2O_3 fibers in the presence of different scavengers, *i.e.* TEMPOL for $^{\bullet}O_2^-$, sodium oxalate for h^+, 2-propanol for $^{\bullet}OH$, and L-tryptophan for $^1O_2$.

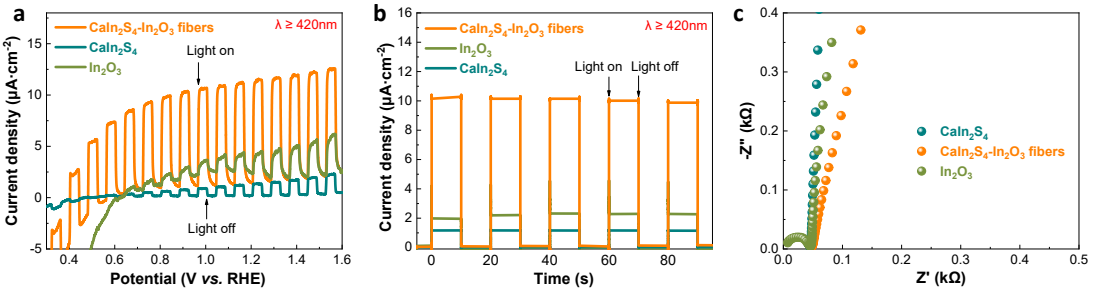

Figure S12. (a) Linear sweep voltammetry (LSV) of $CaIn_2S_4$-In_2O_3 fibers, $CaIn_2S_4$, and In_2O_3 fibers under chopped visible light illumination ($\lambda \geq 420$ nm); (b) transient photocurrent of $CaIn_2S_4$-In_2O_3 fibers, $CaIn_2S_4$, and In_2O_3 fibers; (c) Electrochemical impedance spectra of $CaIn_2S_4$-In_2O_3 fibers, $CaIn_2S_4$, and In_2O_3 fibers.

Table S1. Comparison of disinfection activity for previously reported materials.

Materials	Time (min)	*E. coli* Cell Densuty (CFU / mL)	Catalyst Dosage (mg / mL)	Light source (λ / nm)	Inactivation	Ref.
Graphene Oxide/g-C_3N_4	120	1.0×10^7	0.10	300 W Xe lamp ($\lambda \geq 420$)	7.0 log	[1]
$CuBi_2O_4/Bi_2MoO_6$	240	1.0×10^7	0.80	300 W Xe lamp ($\lambda \geq 420$)	7.0 log	[2]
Ag QDs/$Bi_2S_3/SnIn_4S_8$	240	2.5×10^7	0.60	300 W Xe lamp ($\lambda \geq 420$)	7.3 log	[3]
$MgTi_2O_5$/g-C_3N_4	180	1.0×10^7	0.50	300 W Xe lamp ($\lambda \geq 400$)	7.0 log	[4]
MoS_2 QDs/Bi_2WO_6	90	1.0×10^6	1.00	300W halogen tungsten projector lamp ($\lambda \geq 410$)	6.0 log	[5]
g-C_3N_4/m-Bi_2O_4	90	1.0×10^6	0.40	300 W Xe lamp ($\lambda \geq 400$)	6.0 log	[6]
Ag_2S/g-C_3N_4	90	1.0×10^7	0.80	300 W Xe lamp ($\lambda \geq 420$)	7.0 log	[7]
Graphene/CdS	60	1.0×10^7	0.20	350 W Xe lamp ($\lambda \geq 420$)	5.3 log	[8]
$AgInS_2/TiO_2$	180	$1.0 \times 10^{7.2}$	0.10	300 W Xe lamp ($325 \leq \lambda \leq 845$)	7.2 log	[9]
$InVO_4/AgVO_3$	30	1.0×10^6	0.50	800 W Xe lamp ($\lambda \geq 420$)	6.0 log	[10]
$CaIn_2S_4$-In_2O_3 fibers	20	1.0×10^7	0.50	300 W Xe lamp ($\lambda \geq 400$)	7.0 log	This work

Table S2. Summary of fitted decay lifetime τ and their relative amplitude from the time-resolved photoluminescence decay spectra

Sample	Electron lifetime			Relative amplitude			Average lifetime	χ^2
	τ_1 (ns)	τ_2 (ns)	τ_3 (ns)	A_1 (%)	A_2 (%)	A_3 (%)	τ_a (ns)	
In_2O_3	16.63	163.25	1394.00	5.46	23.23	71.31	1347.60	1.06
$CaIn_2S_4$@In_2O_3	71.90	331.70	1980.00	4.99	22.93	72.08	1892.26	0.98

The average lifetime is calculated by Equation (1):

$$\tau_a = \frac{A_1\tau_1^2 + A_2\tau_2^2 + A_3\tau_3^2}{A_1\tau_1 + A_2\tau_2 + A_3\tau_3} \quad (1)$$

References

1. L. Sung, T. Du, C. Hu, J. N. Chen, J. Lu, Z. C. Lu and H. Y. Han, Antibacterial Activity of Grophene Oxide/g-C3N4 Composite through Photocatalytic Disinfection under Visible Light, *Acs Sustain Chem Eng*, 2017, **5**, 8693-8701.
2. H. X. Shi, J. Fan, Y. Y. Zhao, X. Y. Hu, X. Zhang and Z. S. Tang, Visible light driven CuBi2O4/Bi2MoO6 p-n heterojunction with enhanced photocatalytic inactivation of E. coli and mechanism insight, *J Hazard Mater*, 2020, **381**, 121006.
3. H. Shi, C. Wang, Y. Zhao, E. Liu, J. Fan and Z. Ji, Highly efficient visible light driven photocatalytic inactivation of E. coli with Ag QDs decorated Z-scheme Bi2S3/SnIn4S8 composite, *Appl Catal B-Environ*, 2019, **254**, 403-413.
4. Z. F. Jiang, B. Wang, Y. Li, H. S. Chan, H. L. Sun, T. Q. Wang, H. M. Li, S. Q. Yuan, M. K. H. Leung, A. H. Lu and P. K. Wong, Solar-light-driven rapid water disinfection by ultrathin magnesium titanate/carbon nitride hybrid photocatalyst: Band structure analysis and role of reactive oxygen species, *Appl Catal B-Environ*, 2019, **257**, 117898.
5. X. C. Meng, Z. Z. Li, H. M. Zeng, J. Chen and Z. S. Zhang, MoS2 quantum dots-interspersed Bi2WO6 heterostructures for visible light-induced detoxification and disinfection, *Appl Catal B-Environ*, 2017, **210**, 160-172.
6. S. F. Chang, Y. W. Hu, J. Qian, Y. L. Shao, S. Ni, L. L. Kong, W. Y. Dan, C. Luo, S. Jin and X. X. Xu, Mg2TiO4 spinel modified by nitrogen doping as a Visible-Light-Active photocatalyst for antibacterial activity, *Chem Eng J*, 2021, **410**, 128410.
7. W. Y. Zuo, L. Liang, F. G. Ye and S. L. Zhao, Construction of visible light driven silver sulfide/graphitic carbon nitride p-n heterojunction for improving photocatalytic disinfection, *Chemosphere*, 2021, **283**, 131167.
8. W. J. Wang, T. W. Ng, W. K. Ho, J. H. Huang, S. J. Liang, T. C. An, G. Y. Li, J. C. Yu and P. K. Wong, CdIn2S4 microsphere as an efficient visible-light-driven photocatalyst for bacterial inactivation: Synthesis, characterizations and photocatalytic inactivation mechanisms, *Appl Catal B-Environ*, 2013, **129**, 482-490.
9. J. G. Du, S. L. Ma, H. P. Liu, H. C. Fu, L. Li, Z. Q. Li, Y. Li and J. G. Zhou, Uncovering the

mechanism of novel AgInS2 nanosheets/TiO2 nanobelts composites for photocatalytic remediation of combined pollution, *Appl. Catal. B-Environ.*, 2019, **259**, 118062.

10. H. L. Yan, L. Z. Liu, R. Wang, W. X. Zhu, X. Y. Ren, L. P. Luo, X. Zhang, S. J. Luo, X. L. Ai and J. L. Wang, Binary composite MoS2/TiO2 nanotube arrays as a recyclable and efficient photocatalyst for solar water disinfection, *Chem Eng J*, 2020, **401**, 126052.